Energy & Environmental Science

Cite this: DOI: 10.1039/c1ee02120f

www.rsc.org/ees

PAPER

Plasmon resonant enhancement of dye sensitized solar cells†

Wenbo Hou,[a] Prathamesh Pavaskar,[b] Zuwei Liu,[c] Jesse Theiss,[b] Mehmet Aykol[b] and Stephen B. Cronin*[abc]

Received 12th July 2011, Accepted 26th August 2011
DOI: 10.1039/c1ee02120f

We report an improvement in the efficiency of dye sensitized solar cells (DSSCs) by exploiting the plasmonic resonance of Au nanoparticles. By comparing the performance of DSSCs with and without Au nanoparticles, we demonstrate a 2.4-fold enhancement in the photoconversion efficiency. Enhancement in the photocurrent extends over the wavelength range from 460 nm to 730 nm. The underlying mechanism of enhancement is investigated by comparing samples with different geometries, including nanoparticles deposited on top of and embedded in the TiO_2 electrode, as well as samples with the light absorbing dye molecule deposited on top of and underneath the Au nanoparticles. The mechanism of enhancement is attributed to the local electromagnetic response of the plasmonic nanoparticles, which couples light very effectively from the far field to the near field at the absorbing dye molecule monolayer, thereby increasing the local electron–hole pair (or exciton) generation rate significantly. The UV-vis absorption spectra and photocurrent spectra provide further information regarding the energy transfer between the plasmonic nanoparticles and the light absorbing dye molecules. Based on scanning electron microscope images, we perform electromagnetic simulations of these different Au nanoparticle/dye/TiO_2 configurations, which corroborate the enhancement observed experimentally.

1. Introduction

Since the dye-sensitized solar cell (DSSC) was first demonstrated by O'Regan and Grätzel in 1991,[1] scientists have been working on improving its performance. Several methods, including novel sensitizers,[2–7] electrolytes,[8–10] and semiconductors,[11–13] have been utilized to enhance the power conversion efficiency of DSSCs during the past two decades. However, no significant improvements in efficiency have been made, and the best efficiency is still below 12%. The plasmon resonance of noble metal nanoparticles has become an important area of research with applications in surface-enhanced Raman spectroscopy,[14] nonlinear optical process,[15,16] sub-wavelength photolithography,[17] optical antennas,[18] and TiO_2

[a]*Department of Chemistry, University of Southern California, Los Angeles, CA, 90089, USA. E-mail: scronin@usc.edu*
[b]*Department of Electrical Engineering, University of Southern California, Los Angeles, CA, 90089, USA*
[c]*Department of Physics, University of Southern California, Los Angeles, CA, 90089, USA*

† Electronic supplementary information (ESI) available: Short-circuit photocurrents, photocurrent spectra, absorption spectra of bare TiO_2, Au nanoparticles embedded in TiO_2 without dye molecules; the photovoltaic performance of 5 nm Au thin film without the second annealing deposited between the TiO_2 layer and the dye monolayer as the working electrode; equations used for the calculation of photovoltaic performances of different working electrodes. See DOI: 10.1039/c1ee02120f

Broader context

Dye-sensitized solar cells (DSSCs) have attracted much attention, since their first demonstration by O'Regan and Grätzel in 1991. However, their relatively low efficiencies have not been improved significantly during the past two decades. In this article, we observe a 240% enhancement in the photoconversion efficiency of DSSCs under 532 nm wavelength illumination due to the intense local electromagnetic fields created by the surface plasmons of the Au nanoparticles. These nanoparticles couple light very effectively from the far-field to the near-field, where it can be absorbed by the dye monolayer. The enhancement in photocurrent extends from 460 nm all the way out to the near infrared (730 nm), and reaches a maximum value of 6.5× at a wavelength of 613 nm. The underlying mechanism of enhancement is established by comparing samples with different geometries, including nanoparticles deposited on top of and embedded in the TiO_2 electrode, as well as samples with the light absorbing dye molecule deposited on top of and underneath the Au nanoparticles. This is a major result that may open new degrees of freedom in the optimization strategy of photovoltaics, which, to date, has been too expensive and inefficient to find broad applicability in our energy infrastructure.

photocatalysis.[19,20] For photocatalysis, the large electric fields produced near the surface of metal nanoparticles can be used to accelerate sub-bandgap electron-hole pair generation in TiO_2 catalysts, thereby enhancing the photoconversion efficiency in the visible wavelength range.[19,20] Several attempts have been made to employ noble metal nanoparticles to increase the efficiency of DSSCs.[21–25] In these previous studies, the enhanced efficiency of the DSSC was attributed to the Schottky barrier formed at the metal-semiconductor interface.[21–23,25] In other works, a decreased efficiency was observed with the addition of metal nanoparticles, and attributed to the decreased surface area of the underlying semiconductor in direct contact with the absorbing dye molecules.[24] To date, metal nanoparticle plasmon enhanced DSSCs are still open study.

In this paper, different geometric configurations of Au nanoparticles/dye/TiO_2 are investigated as the working electrode in a DSSC. The relative performances of these geometric configurations enable us to identify and rule out several key aspects of the underlying enhancement mechanism, such as charge transfer, annealing, and surface area. Comparing the UV-vis absorption with the spectral response of the photocurrent provides further information regarding the energy transfer between the plasmonic nanoparticles and the absorbing dye molecules. Electromagnetic simulations of these geometric configurations (based on electron microscope images) corroborate the enhancement observed experimentally.

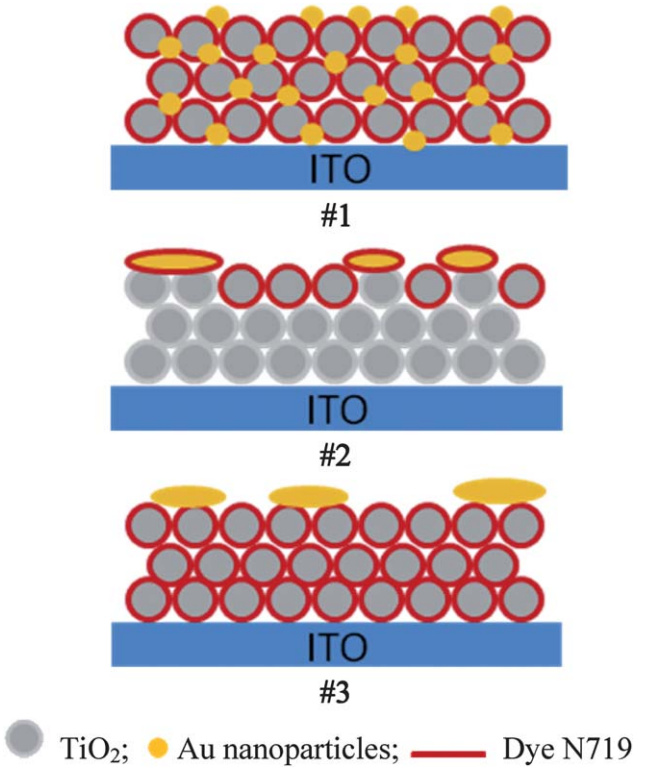

Fig. 1 Schematic diagrams of three different Au nanoparticle/dye/TiO_2 configurations.

2. Experimental

Three basic working electrode configurations with different geometric structures are fabricated and characterized: **#1)** a monolayer of Ru dye N719 deposited on top of Au nanoparticles embedded in a TiO_2 film, **#2)** a monolayer of Ru dye N719 on top of an evaporated 5 nm Au-island thin film deposited on the TiO_2 layer, **#3)** an evaporated 5 nm Au-island thin film deposited on top of the dye monolayer and the TiO_2 layer. Schematic illustrations of these three sample configurations are given in Fig. 1. The conventional DSSC with a monolayer of Ru dye N719 on top of TiO_2 is also prepared as a control. Anatase titania films are prepared in our lab by the sol–gel process and follow the general recipe of acid catalyzing dilute titanium ethoxide in ethanol.[26] The solution is then mixed with surfactant (P123) and stirred for several hours until a sol forms. ITO substrates are spin-coated to achieve the desired film thickness. The substrates are then positioned horizontally and dried at room temperature in air for 24 h, thereby allowing most of the solvents and hydrochloric acid to evaporate and the surfactant to self-organize. The dried films are then annealed at 400 °C for 4 h in air to improve their crystallinity and drive off any remaining solvents and surfactant. For Sample **#1**, Au nanoparticles are embedded in the TiO_2 films using a modified recipe described by Li *et al.*[27] In this recipe, P 123, titanium ethoxide, and $HAuCl_4$ are mixed in the ethanol at room temperature and spin-coated on ITO substrates. After aging at 40 °C for 24 h and 100 °C for 12 h, the gels are calcined at 350 °C for 4 h in air using a heating rate of 0.5 °C/min. In order to prepare Sample **#2**, a gold film with a nominal thickness of 5 nm is evaporated on the top of the sol–gel TiO_2 film. A second annealing process is carried out by placing the sample into a furnace and calcining in air at 400 °C for 1 h. The 5 nm evaporated Au films are not thick enough to form a continuous film of Au, and instead form island-like growth, as shown in Fig. 2a. The second annealing process makes these islands more spherical, as shown in Fig. 2b. These thin Au films serve as good substrates for surface enhanced Raman spectroscopy (SERS) and other plasmonic phenomena.[28,29] The conventional DSSC and Samples **#1** and **#2** are then sensitized by immersing into a 0.3 mM solution of N719 dye in ethanol. All samples are sensitized for 48 h. In order to make Sample **#3**, a gold film with a nominal thickness of 5 nm is evaporated on top of the dye surface of the conventional DSSC. Absorption spectra of all working electrodes are recorded on a Perkin-Elmer Lambda 950 UV/Vis/NIR spectrophotometer with an integrating sphere detector. For the counter electrode, a 10 nm film of Pt is deposited by electron-beam evaporation onto ITO. The working electrode and the counter electrode are separated by a polypropylene spacer approximately 20 μm thick and bonded using binder clips. The internal space of the cells is filled with electrolyte (Iodolyte AN-50 from Solaronix) and sealed with hot-melt sealing foil (Meltonix 1170-25 from Solaronix). The open-circuit photovoltage, short-circuit photocurrent, and *I–V* characteristics of these solar cells are measured using a digital multimeter (Keithley 2400). A fixed wavelength green laser (60 mW, 532 nm) is employed to illuminate the solar cells. In addition, the spectral response of the photocurrent is measured using a Fianium supercontinuum white light laser in conjunction with a Princeton Instruments double grating monochromator.

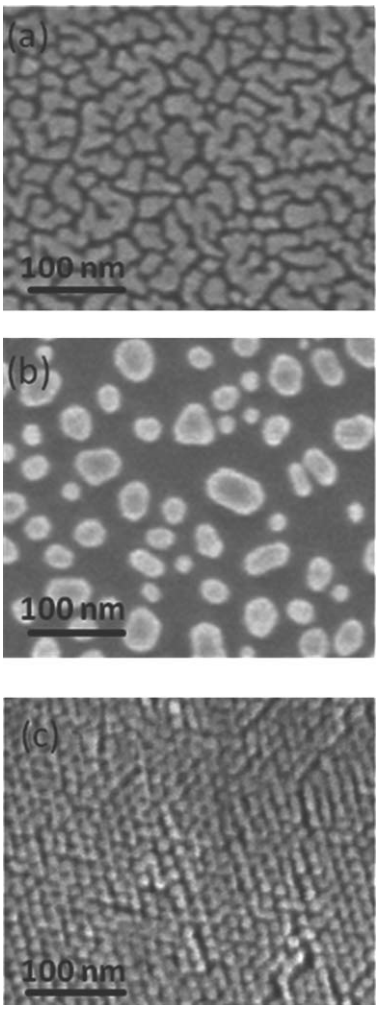

Fig. 2 (a) SEM image of 5 nm Au thin film before the second annealing. (b) SEM image of 5 nm Au thin film after the second annealing. (c) SEM image of TiO_2 film with a mesoporous structure.

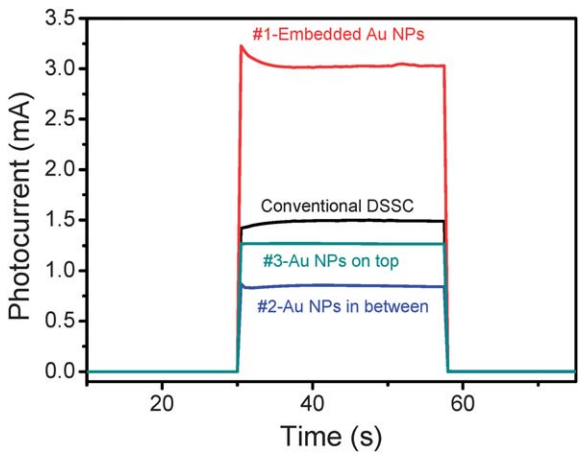

Fig. 3 Short-circuit photocurrents of DSSCs with three different Au nanoparticle/dye/TiO_2 configurations.

3. Results and discussion

3.1. Short-circuit photocurrents

Fig. 3 shows the short-circuit photocurrent during a 28-second laser exposure at a wavelength of 532 nm. Under illumination, the highest photocurrent is produced by working electrode **#1** (dye monolayer deposited on top of embedded Au nanoparticles/TiO_2). Comparing this with the photocurrent produced by the conventional DSSC, the photocurrent increased by a factor of 2. This enhancement is due to the intense local electromagnetic fields produced by the plasmonic nanoparticles, which couple light very effectively from the far-field to the near-field of the dye molecule monolayer. Under these intense local fields, the exciton generation rate in the dye molecule monolayer increases significantly, thereby improving the photocurrent. The photocurrents produced by **#2** and **#3**, however, are lower than that of the conventional DSSC, even with the addition of Au nanoparticles. The decrease in photocurrent, here, is attributed to the following facts. (1) For **#2**, the 5 nm Au thin film is deposited between the TiO_2 film and the dye monolayer. The Au thin film, therefore, decreases the active surface area of TiO_2 in direct contact with the dye molecules. This decrease also demonstrates that charge is not transferring from the dye to the Au or from the Au to the TiO_2. That is, in order for this solar cell to function properly, the charge must be created in the dye layer and then transferred to the TiO_2 and surrounding electrolyte solution. Even though the plasmon enhancement partially compensates for the decrease in photocurrent caused by the reduced contact area between the dye and TiO_2, the photocurrent produced by **#2** is still lower than that of the conventional DSSC. As a control experiment, we also prepared a sample with a 5 nm Au thin film without the second annealing process between the TiO_2 layer and the dye monolayer. The photocurrent produced by this control sample (0.34 mA) is lower than that produced by **#2** (0.86 mA), as shown in Figure S1 in the supplemental document.† This is because the Au islands in the 5 nm film tend to cluster and form more spherical nanoparticles after annealing, as shown in Fig. 2b, and therefore do not cover as much of the TiO_2 surface area. (2) For **#3**, the 5 nm Au thin film lies on the top of the dye monolayer. For this geometric structure, less dye can absorb the light since the Au thin film covers about 40% surface area of the dye (see Fig. 2b). Therefore, while Samples **#1**, **#2**, and **#3** all consist of Au nanoparticles/dye/TiO_2 working electrodes, the effectiveness of the plasmon-enhancement depends on the specific geometric configuration of these three constituent materials.

Anatase TiO_2 prepared by the acid catalyzing sol–gel process has a hexagonal close packed mesoporous structure, as shown in Fig. 2c.[26] In the plasmon enhanced configuration, the Au nanoparticles sit in the pores of the TiO_2. These embedded Au nanoparticles not only create intense local fields, but also maintain most of the contact area between the dye and the TiO_2. The photocurrents of bare TiO_2 and Au nanoparticles embedded in TiO_2 are also measured as a control. No photocurrents are observed for these two samples, as expected, since no dye molecule is deposited. This result further confirms that the plasmon excited electrons are not able to transfer directly from the Au nanoparticles to the TiO_2, consistent with our previous

work on plasmon-enhanced photocatalysis.[19,20] In contrast to our previous work, however, doping and defects in the TiO_2 do not affect the DSSC performance, since the electron-hole pairs are generated in the dye rather than the TiO_2.[19,20]

3.2. Photocurrent spectra

Fig. 4a shows the photocurrent spectra of DSSCs with the four different working electrodes. Sample **#1** shows a large enhancement in photocurrent with respect to the conventional DSSC over most of the visible wavelength range. The inset in Fig. 4a shows the photocurrent enhancement ratio of Sample **#1** with respect to the conventional DSSC. We observe enhancement from 460 nm all the way out to the near infrared (730 nm). This enhancement ratio peaks at 6.5 at wavelengths of 613 nm. The peak photocurrents for **#1** (red dashed curve), and **#2** (blue dotted curve) are redshifted with respect to the conventional DSSC (dark solid curve). This redshift is caused by the plasmonic enhancement, which has a maximum around 566 nm, as shown in Figure S2a of the supplemental document.† The overall photocurrents of samples **#2** and **#3** are lower than the conventional DSSC for the same reasons given above, namely the decreased effective area of the dye molecule monolayer.

In order to understand the performance of these solar cells, spherically integrated UV-vis absorption spectra of the four working electrodes are measured, and are shown in Fig. 4b. The absorption of the conventional DSSC (black solid curve) peaks around 510 nm due to the absorption of the dye. With the addition of Au nanoparticles, this absorption increases further and redshifts to 530 nm (red dashed curve) because the plasmonic Au nanoparticles couple the light more effectively in this region of the electromagnetic spectrum and improve the light absorption of the dye. The absorption of **#2** and **#3** are lower than the absorption of the conventional DSSC due to the decrease in dye-coated surface area. The absorption of **#1** and **#3** are bigger than that of **#2**, since the plasmonic Au nanoparticles absorb light most effectively in **#1** and **#3** due to their geometric configuration. It is for this reason that **#1** can create the highest photocurrent. However, in **#3**, the dye layer is covered by the Au thin film. Consequently, approximately 40% of the dye surface area is covered by the Au nanoparticles and cannot absorb the incident light effectively. The photocurrent produced by **#3** is still lower than that of the conventional DSSC. Note that the UV-vis absorption of **#1** and the conventional DSSC are comparable, while the photocurrent of **#1** is much greater than the conventional DSSC. This is because the plasmonic near-field absorption dominates the photocurrent behavior, while bulk (far-field) absorption dominates the UV-vis response.

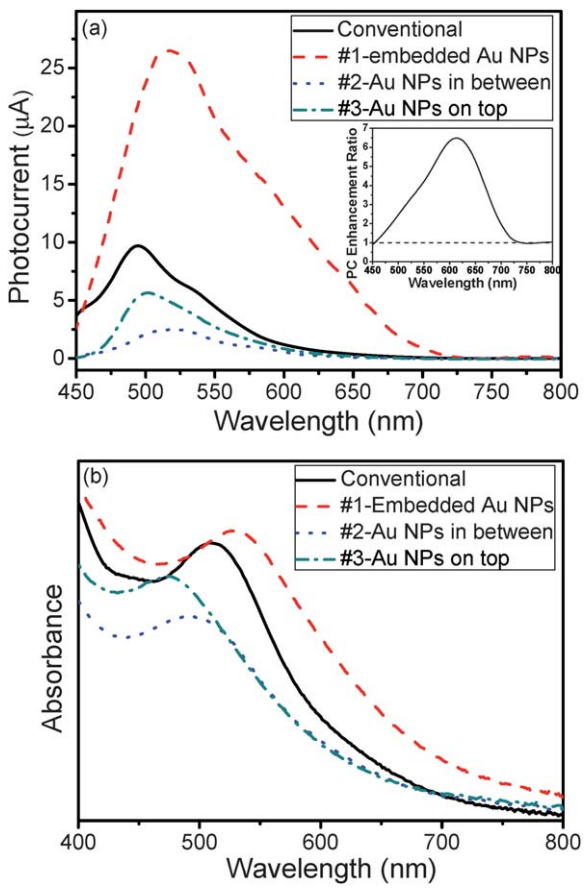

Fig. 4 (a) Photocurrent spectra of DSSCs with different working electrodes. (b) Absorption spectra of different working electrodes.

Two control samples were also measured, a bare TiO_2 film prepared by the sol–gel method and Au nanoparticles embedded in TiO_2 with no dye molecule. Figure S2 in the supplemental document† shows the UV-vis spectra and photocurrent spectra taken for these two control samples. The bare TiO_2 UV-vis spectrum shows transparency for wavelengths above 450 nm. Correspondingly, no photocurrent is observed for this sample under visible illumination, as shown in Figure S2b. The absorption spectrum taken from Au nanoparticles embedded in TiO_2 (red dashed curve in Figure S2a) exhibits a peak in the absorption around 566 nm, corresponding to the plasmon resonance of the Au nanoparticles, although the absorption of this film is quite broad due to its inhomogeneity.[30] While this sample absorbs light in the visible range, it does not produce a photocurrent (Figure S2b) since no dye molecule is present to initiate electron-hole generation.

3.3. *I–V* curves and photoconversion efficiencies

Fig. 5 shows the typical *I–V* curves for the four solar cells under 532 nm wavelength laser illumination. Table 1 summarizes this

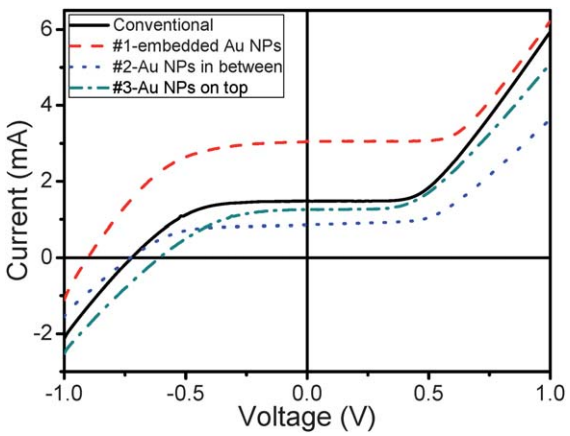

Fig. 5 *I–V* characteristics of DSSCs with different working electrodes.

Table 1 Summary of photovoltaic device performances

Working electrode	V_{oc} (V)	I_{sc} (mA)	FF (%)	η (%)
Conventional	0.72	1.48	53	0.94
#1	0.83	3.04	54	2.28
#2	0.73	0.86	58	0.60
#3	0.61	1.26	46	0.58

data, listing the open-circuit photovoltages, short-circuit photocurrents, fill factors, and overall power conversion efficiencies. The equations used to calculate fill factors and photoconversion efficiencies are given in the supplemental document.† The DSSC made of **#1** gives the highest performance of 2.28% conversion efficiency. It should be noted, however, that these samples are intended for proof-of-principle purposes, and have not been optimized for overall photoconversion efficiency. We believe the photoconversion efficiencies will be much higher after optimization, for example, thicker TiO_2 layer. The conventional DSSC made of TiO_2 without Au nanoparticles gives an efficiency of 0.94%. The performance of this DSSC is improved by 2.4 times due to the plasmonic enhancement. However, devices **#2** and **#3** show lower performances than the conventional DSSC either due to the reduced effective area of TiO_2 in contact with the dye molecules or the decreased dye area exposed to the light by Au nanoparticle layer, as discussed above. In addition, we found that the second annealing process is very important to form strongly plasmonic Au nanoparticles in Sample **#2**. As a control experiment, the efficiency of device **#2** without the second annealing process is also measured (0.14% in Table S1 of the supplemental document†). This is more than 4 times smaller than the efficiency of device **#2** (0.60%).

3.4. FDTD simulations

Fig. 6 shows the calculated enhancement factors due to Au nanoparticles. These results were calculated using full three-dimensional finite difference time domain (FDTD) simulations of the different Au nanoparticle geometries studied experimentally. The enhancement factors were calculated as ratios of the absorption cross-sections in the sol–gel TiO_2 with and without Au nanoparticles. The dielectric function used for Au was derived from the data by Palik and Ghosh.[31] The dielectric constant of the sol–gel TiO_2 was calculated using the Maxwell Garnett effective medium theory due to its mesoporous geometry.[32] The enhancement factor for the embedded Au nanoparticles in Fig. 6 shows a well defined peak with an enhancement of 9, which is of the order of the experimental value of 6.5. There is little to no enhancement in the case of Au nanoparticles deposited on top of the TiO_2, which also agrees well with the experimentally observed results shown in Fig. 4. Here, it should be noted that the absorption was calculated over a 100 nm thick volume of TiO_2, whereas in our previous article it was calculated over only a 10 nm thick volume, as limited by the minority carrier diffusion length of the TiO_2. This more accurately reflects the porous sample topography of the dye-TiO_2 interface. The lack of enhancement calculated in the case of Au nanoparticles deposited on top of TiO_2 is due to the local electric fields produced by the nanoparticles, which do not penetrate deep enough to provide a net enhancement over this volume.

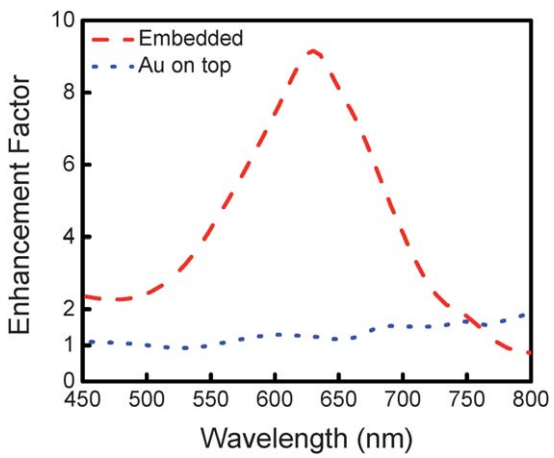

Fig. 6 FDTD calculated enhancement factor plotted as a function of wavelength for embedded nanoparticles and Au nanoparticles on top of TiO_2 with respect to the conventional DSSC.

4. Conclusions

In summary, a 2.4-fold plasmonic enhancement in the overall conversion efficiency of DSSCs under visible illumination is observed when Au nanoparticles are embedded in TiO_2. This enhancement is dependent on the geometric configuration of the Au nanoparticles/dye/TiO_2 working electrode. In particular, the embedded Au nanoparticles show an enhancement in the photocurrent over the wavelength range from 460 nm to 730 nm. Conversely, depositing Au nanoparticles on top of the TiO_2 results in a decreased efficiency by reducing the effective area of TiO_2 in contact with dye or by reducing the dye surface area exposed to the light. This efficiency decrease also reveals that direct charge transfer from Au to TiO_2 does not occur, and that the plasmonic enhancement results solely from the local electromagnetic fields. Finally, electromagnetic simulations agree well with the experimental observations, further corroborating the mechanism of plasmonic enhancement in these DSSCs.

Acknowledgements

This research was supported as part of the Center for Energy Nanoscience, an Energy Frontier Research Center funded by the U.S. Department of Energy, Office of Science, Office of Basic Energy Sciences under Award Number DE-SC0001013.

References

1 B. Oregan and M. Gratzel, *Nature*, 1991, **353**, 737.
2 C. Y. Chen, M. K. Wang, J. Y. Li, N. Pootrakulchote, L. Alibabaei, C. H. Ngoc-le, J. D. Decoppet, J. H. Tsai, C. Gratzel, C. G. Wu, S. M. Zakeeruddin and M. Gratzel, *ACS Nano*, 2009, **3**, 3103.
3 F. Gao, Y. Wang, D. Shi, J. Zhang, M. K. Wang, X. Y. Jing, R. Humphry-Baker, P. Wang, S. M. Zakeeruddin and M. Gratzel, *J. Am. Chem. Soc.*, 2008, **130**, 10720.
4 F. F. Gao, Y. Wang, J. Zhang, D. Shi, M. K. Wang, R. Humphry-Baker, P. Wang, S. M. Zakeeruddin and M. Gratzel, *Chem. Commun.*, 2008, 2635.
5 C. Klein, K. Nazeeruddin, D. Di Censo, P. Liska and M. Gratzel, *Inorg. Chem.*, 2004, **43**, 4216.

6 H. Qin, S. Wenger, M. Xu, F. Gao, X. Jing, P. Wang, S. M. Zakeeruddin and M. Gratzel, *J. Am. Chem. Soc.*, 2008, **130**, 9202.
7 M. K. Wang, M. F. Xu, D. Shi, R. Z. Li, F. F. Gao, G. L. Zhang, Z. H. Yi, R. Humphry-Baker, P. Wang, S. M. Zakeeruddin and M. Gratzel, *Adv. Mater.*, 2008, **20**, 4460.
8 Y. Bai, Y. M. Cao, J. Zhang, M. Wang, R. Z. Li, P. Wang, S. M. Zakeeruddin and M. Gratzel, *Nat. Mater.*, 2008, **7**, 626.
9 S. A. Cerneaux, S. M. Zakeeruddin, M. Gratzel, Y. B. Cheng and L. Spiccia, *J. Photochem. Photobiol., A*, 2008, **198**, 186.
10 S. Ito, S. M. Zakeeruddin, P. Comte, P. Liska, D. B. Kuang and M. Gratzel, *Nat. Photonics*, 2008, **2**, 693.
11 J. Chung, J. Myoung, J. Oh and S. Lim, *J. Phys. Chem. C*, 2010, **114**, 21360.
12 M. F. Hossain and T. Takahashi, *Mater. Chem. Phys.*, 2010, **124**, 940.
13 S. Yun, J. Lee, J. Chung and S. Lim, *J. Phys. Chem. Solids*, 2010, **71**, 1724.
14 K. Kneipp, *Phys. Today*, 2007, **60**, 40.
15 M. Danckwerts and L. Novotny, *Optical Phys. Rev. Lett.*, 2007, **98**, 2.
16 K. Chen, C. Durak, J. R. Heflin and H. D. Robinson, *Nano Lett.*, 2007, **7**, 254.
17 W. Srituravanich, N. Fang, C. Sun, Q. Luo and X. Zhang, *Nano Lett.*, 2004, **4**, 1085.
18 M. W. Knight, H. Sobhani, P. Nordlander and N. J. Halas, *Science*, 2011, **332**, 702.
19 W. Hou, Z. Liu, P. Pavaskar, W. H. Hung and S. B. Cronin, *J. Catal.*, 2011, **277**, 149.
20 Z. Liu, W. Hou, P. Pavaskar, M. Aykol and S. B. Cronin, *Nano Lett.*, 2011, **11**, 1111.
21 Z. H. Chen, Y. B. Tang, C. P. Liu, Y. H. Leung, G. D. Yuan, L. M. Chen, Y. Q. Wang, I. Bello, J. A. Zapien, W. J. Zhang, C. S. Lee and S. T. Lee, *J. Phys. Chem. C*, 2009, **113**, 13433.
22 C. S. Chou, R. Y. Yang, C. K. Yeh and Y. J. Lin, *Powder Technol.*, 2009, **194**, 95.
23 W. H. Lai, Y. H. Su, L. G. Teoh and M. H. Hon, *J. Photochem. Photobiol., A*, 2008, **195**, 307.
24 C. K. N. Peh, L. Ke and G. W. Ho, *Mater. Lett.*, 2010, **64**, 1372.
25 Y. H. Su, W. H. Lai, L. G. Teoh, M. H. Hon and J. L. Huang, *Appl. Phys. A: Mater. Sci. Process.*, 2007, **88**, 173.
26 P. C. A. Alberius, K. L. Frindell, R. C. Hayward, E. J. Kramer, G. D. Stucky and B. F. Chmelka, *Chem. Mater.*, 2002, **14**, 3284.
27 H. X. Li, Z. F. Bian, J. Zhu, Y. N. Huo, H. Li and Y. F. Lu, *J. Am. Chem. Soc.*, 2007, **129**, 4538.
28 R. Kumar, H. Zhou and S. B. Cronin, *Appl. Phys. Lett.*, 2007, **91**, 223105.
29 R. P. Vanduyne, J. C. Hulteen and D. A. Treichel, *J. Chem. Phys.*, 1993, **99**, 2101.
30 I. Doron-Mor, Z. Barkay, N. Filip-Granit, A. Vaskevich and I. Rubinstein, *Chem. Mater.*, 2004, **16**, 3476.
31 E. D. Palik and G. Ghosh, *Handbook of optical constants of solids*, Academic Press, 1998.
32 G. A. Niklasson, C. Granqvist and O. Hunderi, *Appl. Opt.*, 1981, **20**, 26.

